Energy Advances

ROYAL SOCIETY OF CHEMISTRY

PAPER

View Article Online
View Journal | View Issue

Cite this: *Energy Adv.*, 2024, 3, 1672

Construction of a supramolecular light-harvesting system based on pillar[5]arene-mediated nanoparticles in water†

Xiuxiu Li,[a] Qiaona Zhang,[a] Xiaoman Dang,[a] Fengyao Cui,[a] Zheng-Yi Li,[a] Xiao-Qiang Sun[b] and Tangxin Xiao *[a]

Received 19th April 2024,
Accepted 20th May 2024

DOI: 10.1039/d4ya00252k

rsc.li/energy-advances

Light harvesting and energy transfer are ubiquitous processes in natural photosynthesis, significantly advancing the widespread utilization of solar energy. In this study, we engineered a supramolecular light-harvesting system utilizing a pyridinium salt-modified cyanostilbene guest (**CPy**) and a water-soluble pillar[5]arene host (**WP5**). Through host–guest complexation between **WP5** and **CPy**, the resultant supra-amphiphile further self-assembled into emissive nanoparticles within aqueous environments. Incorporating the commercially available dye **DBT** into these nanoparticles yielded an efficient artificial light-harvesting system with a high donor/acceptor ratio (>200). Additionally, this system demonstrated tunable fluorescence emission in the solid state and exhibited potential applications as a color-tunable fluorescent ink for information encryption. Our findings not only delineate a promising approach for fabricating efficient light-harvesting systems *via* a straightforward supramolecular strategy but also underscore the significant potential of tunable photoluminescent nanomaterials.

Introduction

Inspired by natural light-harvesting systems,[1–3] scientists are driven to harness renewable energy resources more effectively. These systems, like chloroplasts found in green plants, excel in capturing, transferring, and storing solar energy within nano-sized devices. Moreover, the light-harvesting systems found in chloroplasts are intricate supramolecular organizations of chlorophyll and protein molecules.[4] Taking cues from nature, numerous artificial light-harvesting systems (ALHS) assembled by non-covalent interactions have emerged in recent years for different applications,[5–10] such as photocatalysis,[11–18] tunable luminescent materials,[19–30] chemical sensing,[31–33] bioimaging/therapy,[34–36] temperature sensing,[37–41] information encryption[42–44] and latent fingerprint imaging.[45,46] There are three key conditions to achieve efficient Förster resonance energy transfer (FRET) from an energy donor (D) to an acceptor (A): firstly, a substantial overlap between the absorption spectrum of the acceptor and the emission spectrum of the donor is a prerequisite; secondly, the donor must be densely packed while circumventing aggregation-induced fluorescence quenching (ACQ); thirdly, maintaining a high donor-to-acceptor ratio (D/A > 200) ensures that multiple donors are associated with a single acceptor, optimizing energy transfer efficiency.[47–50]

To mitigate the ACQ effect associated with conventional dyes, the incorporation of aggregation-induced emission (AIE) donors becomes essential.[51–53] In this context, the synergistic integration of AIE with supramolecular self-assembly offers significant advantages for the fabrication of ALHSs.[54–57] Recently, fluorophores based on cyanostilbene (CS) have garnered considerable attention owing to their distinctive fluorescence properties.[58–62] CS derivatives often exhibit weak emission in organic solvents but display remarkable fluorescence in aqueous environments. Consequently, the CS group can serve as an effective AIE unit for the synthesis of various luminescent materials.[63,64] Previously, our research group reported a multicolor fluorescent nanomaterial based on CS groups, demonstrating promising applications in time-dependent information encryption and dual-color latent fingerprint imaging.[65] Furthermore, we integrated CS groups into quadruple hydrogen bonding polymers to engineer an ALHS with an ultralow acceptor content, thereby achieving white-light emission.[66] Notably, supramolecular macrocycles such as pillar[5]arene can be readily converted into water-soluble hosts and possess remarkable capabilities for modulating the emission of guest molecules.[67–70] Thus, the utilization of water-soluble pillar[5]arene to fine-tune CS-based simple guests represents a highly desirable strategy for achieving efficient FRET.

[a] School of Petrochemical Engineering, Changzhou University, Changzhou 213164, China. E-mail: xiaotangxin@cczu.edu.cn
[b] Institute of Urban & Rural Mining, Changzhou University, Changzhou 213164, China

† Electronic supplementary information (ESI) available. See DOI: https://doi.org/10.1039/d4ya00252k

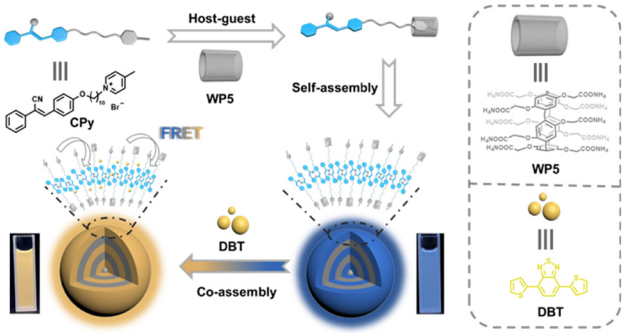

Fig. 1 Schematic representation of the construction of ALHS in water based on **WP5⊃CPy** and **DBT**.

In this work, we devised and synthesized a straightforward guest molecule, denoted as **CPy**, incorporating a methyl pyridinium salt group as the host-binding motif and a CS group as the fluorescence-generating component (Fig. 1). Moreover, the synthesized water-soluble pillar[5]arene, designated as **WP5**, has the capability to form host–guest complexes with **CPy**, yielding a supra-amphiphile denoted as **WP5⊃CPy**. Consequently, **WP5⊃CPy** assemblies give rise to nanoparticles (NPs) in aqueous environments. This assembly not only amplifies the fluorescence intensity of **CPy** but also provides a nanostructured platform conducive to the development of ALHSs. To harness excitation energy from **WP5⊃CPy**, a commercially available fluorescent dye, 4,7-di(2-thienyl)-benzo[2,1,3]thiadiazole (**DBT**), was selected as the acceptor and loaded into the hydrophobic layer of the NPs. This system facilitates an efficient FRET process and exhibits a pronounced antenna effect in aqueous media. Remarkably, this ALHS not only emulates natural light-harvesting systems but also demonstrates significant potential as a fluorescent ink and solid-state luminescent material.

Experimental

All chemicals and reagents were purchased from commercial suppliers and utilized, unless specifically noted otherwise, without additional purification. Solvents, if required, were subjected to dehydration using established procedures outlined in the literature. Isolated yields were reported for all reactions. Proton nuclear magnetic resonance (^{1}H NMR) spectra were acquired using a Bruker AVANCE III spectrometer operating at either 300 MHz or 400 MHz and calibrated relative to the residual proton signal or the natural abundance carbon resonance of the deuterated solvent, with tetramethylsilane (TMS) employed as the internal standard. Chemical shifts (δ) are expressed in parts per million (ppm) and coupling constants (J) are provided in Hz. Multiplicities are denoted as s (singlet), d (doublet), t (triplet), and m (multiplet). High-resolution electrospray ionization mass spectra (HR-ESI-MS) were recorded using an Agilent Technologies 6540 UHD Accurate-Mass spectrometer. Transmission electron microscopy (TEM) investigations were conducted on a JEM-2100 instrument. Dynamic light scattering (DLS) and zeta-potential (ζ-potential) measurements were performed using a Zetasizer Nano ZS ZEN3600 instrument. UV-vis absorption spectra were obtained using a PerkinElmer Lambda 35 UV-vis spectrometer, while fluorescence measurements were conducted on an agilent cary eclipse spectrofluorometer. Fluorescence lifetimes were determined using time-correlated single photon counting on an FLS980 instrument equipped with a pulsed xenon lamp. The fluorescence decay curves were fitted using a bi-exponential decay model. The instrument response function (IRF) measures the scattering of laser excitation from non-fluorescent control samples to ascertain the fastest possible response of the detectors. Quantum yield measurements were conducted using an FLS980 instrument with an integrating sphere. The CIE (Commission Internationale de l'Eclairage) 1931 coordinates were calculated with the method of color matching functions.

The macrocyclic host, **WP5**, is a water-soluble pillar[5]arene, synthesized following established procedures outlined in the literature.[71] The synthesis of the guest molecule **CPy** is depicted in Scheme 1. Initially, 4-hydroxyphenylacetonitrile undergoes etherification with 1,10-dibromodecane to yield compound **1**. Then, compound **1** undergoes condensation with benzaldehyde *via* a Knoevenagel reaction, resulting in the formation of compound **2**. Finally, compound **2** reacts with 4-methylpyridine through nucleophilic substitution, culminating in the synthesis of the target product, **CPy**. Synthesis of compound **1** was carried out based on literature methods.[72] Compound **2** and **CPy** were thoroughly characterized using ^{1}H NMR, ^{13}C NMR, and high-resolution electrospray ionization mass spectrometry (ESI-MS) techniques (Fig. S1–S6, ESI†).

Synthesis of compound **2**. Compounds **1** (0.50 g, 1.4 mmol) and ^{t}BuOK (0.16 g, 1.4 mmol) were introduced into a 250 mL three-neck flask under a nitrogen atmosphere. Subsequently, anhydrous ethanol (75 mL) was added. Once the solid was completely dissolved, benzaldehyde (0.18 g, 1.7 mmol) was gradually added. The resulting mixture was stirred at room temperature for 3 h. Upon completion of the reaction, the solid was retained following extraction and filtration, yielding white solid compound **2** (0.49 g, 1.1 mmol) with a yield of 78%. ^{1}H NMR ($CDCl_3$, 300 MHz, 298 K) δ (ppm): 7.86 (d, J = 7.2 Hz, 2H, Ar-*H*), 7.60 (d, J = 8.4 Hz, 2H, Ar-*H*), 7.35 (m, 4H, Ar-*H* and –C*H*═C(CN)–), 6.95 (d, J = 8.4 Hz, 2H, Ar-*H*), 4.00 (t, J = 6.3 Hz, 2H, –OCH_2), 3.41 (t, J = 6.9 Hz, 2H, –BrCH_2–), 1.91–1.80 (m, 4H, –CH_2–), 1.78–1.33 (m, 12H, –CH_2–). ^{13}C NMR ($CDCl_3$, 100 MHz, 298 K) δ (ppm): 160.06, 140.00, 134.03, 130.13, 129.07, 128.93, 127.32, 126.75, 118.21, 114.97, 111.38, 68.21, 34.10, 32.83,

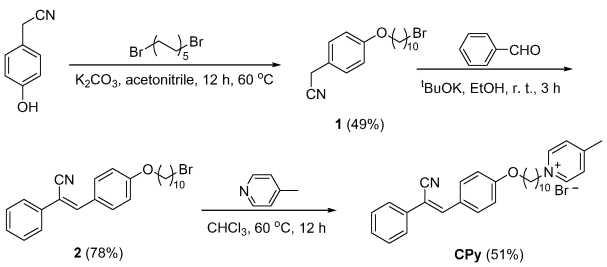

Scheme 1 Synthetic route of **CPy**.

29.73, 29.45, 29.38, 29.19, 28.76, 28.18, 26.01. HR-ESI-MS: *m*/*z* $[M + Na]^+$ calcd for $[C_{25}H_{30}BrNNaO]^+$ 462.1403, found 462.1403.

Synthesis of **CPy**. Compound **2** (0.50 g, 1.1 mmol) and 4-methylpyridine (1.48 g, 15.9 mmol) were combined in a 50 mL flask. Anhydrous chloroform (30 mL) was then added, and the mixture was stirred at 60 °C for 12 h. Upon completion of the reaction, the solvent was evaporated under reduced pressure. The resulting residue underwent column chromatography (eluent: PE : EA = 1 : 1, MeOH : H_2O = 10 : 1, v/v), yielding a pure brown solid compound **CPy** (0.30 g, 0.56 mmol) with a yield of 51%. ^{1}H NMR (300 MHz, DMSO-d_6, 298 K) δ (ppm): 8.93 (d, J = 6.0 Hz, 2H, Ar-*H*), 7.98 (d, J = 6.0 Hz, 2H, Ar-*H*), 7.92–7.89 (m, 3H, Ar-*H* and –C*H*═C(CN)–), 7.69 (d, J = 8.7 Hz, 2H, Ar-*H*), 7.55–7.47 (m, 3H, Ar-*H*), 7.05 (d, J = 8.7 Hz, 2H, Ar-*H*), 4.51 (t, J = 7.2 Hz, 2H, –NCH_2–), 4.02 (t, J = 6.3 Hz, 2H, –OCH_2–), 2.60 (s, 3H, –CH_3), 1.88 (m, 2H, –CH_2–), 1.71 (m, 2H, –CH_2–), 1.40–1.22 (m, 12H, –CH_2–). ^{13}C NMR δ (100 MHz, DMSO-d_6, 298 K) δ (ppm): 159.50, 158.73, 143.69, 140.50, 133.96, 130.21, 128.91, 128.87, 128.32, 127.20, 125.93, 118.03, 115.02, 109.95, 67.66, 59.87, 30.55, 28.83, 28.69 (2C), 28.56, 28.33, 25.44, 25.35, 21.33. HR-ESI-MS: *m*/*z* $[M–Br]^+$ calcd for $[C_{31}H_{37}N_2O]^+$ 453.2901, found 453.3575.

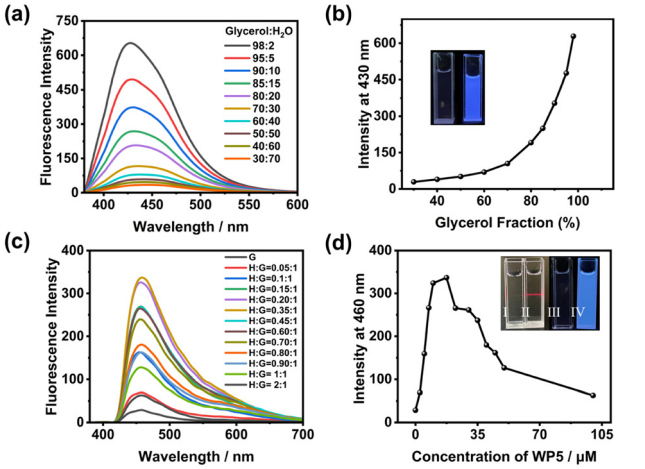

Fig. 2 (a) Fluorescence spectra of **CPy** (1×10^{-4} M) in a glycerol/water solution with different fractions of glycerol (λ_{ex} = 360 nm). (b) Fluorescence intensity of **CPy** at 430 nm in the presence of different factions of glycerol from 30 to 98%; inset: photographs of **CPy** in water (left) and in glycerol (right, with 2% water) under a turn-on UV lamp. (c) Fluorescence spectra of **CPy** (as the guest, G, 5×10^{-5} M) in pure water upon the titration of **WP5** (as the host, H). (d) Fluorescence intensity of **CPy** (5×10^{-5} M) at 460 nm *versus* different concentrations of WP5; insets: Tyndall effects of **CPy** (I) and **WP5**⊃**CPy** (II), and fluorescence photographs of **CPy** (III) and **WP5**⊃**CPy** (IV).

Results and discussion

The AIE behavior of **CPy** in mixed solvents was initially explored. In pure water, **CPy** dissolved completely and exhibited no fluorescence emission. Upon the addition of a poor solvent, glycerol, the fluorescence of **CPy** at 430 nm gradually increased (Fig. 2a and b). A sharp increase in fluorescence was observed when the glycerol fraction reached 98%. Despite the amphiphilic nature of **CPy**, attempts to determine its critical aggregation concentration (CAC) in water through optical transmittance experiments (Fig. S7, ESI†) were inconclusive, indicating the absence of a distinct CAC within this concentration range. The aggregation of **CPy** molecules in mixed solvents appeared to be disordered and challenging to control. Based on these observations, we further endeavored to investigate the aggregation and luminescence of **CPy** through supramolecular self-assembly to achieve well-ordered nanostructures.

WP5 was employed to facilitate the self-assembly of **CPy** through host–guest interactions in pure water. Upon the addition of **WP5** to the **CPy** solution (5×10^{-5} M), a notable enhancement in the fluorescence intensity of **CPy** was observed (Fig. 2c), indicating the effective induction of **CPy** self-assembly by **WP5** in water. The fluorescence intensity reached its maximum when the **WP5** concentration was 17.5 μM, suggesting an optimal molar ratio of **WP5** to **CPy** of 0.35 : 1 (Fig. 2d). Additionally, a distinct Tyndall effect was observed for **WP5**⊃**CPy**, confirming the presence of abundant NPs in the solution (Fig. 2d, inset). Notably, the CAC of **WP5**⊃**CPy** was determined to be 2.5 μM (Fig. S8, ESI†). In the presence of **WP5**, the absolute fluorescence quantum yield of **CPy** increased significantly to 2.72%, underscoring the pivotal role of **WP5** in fluorescence enhancement (Fig. S10a, ESI†).

The morphology and size of the **WP5**⊃**CPy** nanostructures were characterized using transmission electron microscopy (TEM) and dynamic light scattering (DLS). DLS analysis revealed a narrow size distribution for **WP5**⊃**CPy**, with an average hydrodynamic diameter of 142 nm (Fig. 3a). TEM imaging depicted spherical nanoaggregates with a diameter of approximately 100 nm, consistent with the DLS data (Fig. 3c). As **WP5**⊃**CPy** NPs exhibited pronounced fluorescence in pure water, efforts were made to construct a donor–acceptor system by co-assembling hydrophobic ACQ dyes into the NPs. To this end, the commercially available dye **DBT** was chosen due to its well-matched photophysical spectra (Fig. 4a). The morphology of **WP5**⊃**CPy-DBT** NPs was also investigated using DLS and TEM, revealing a spherical structure with an average hydrodynamic diameter of 191 nm (Fig. 3b and d). Zeta potential measurements were further conducted for both **WP5**⊃**CPy** (−53 mV) and **WP5**⊃**CPy-DBT** (−36 mV) NPs (Fig. S9, ESI†). The relatively high negative values for both nanoparticles indicate their stability in water, as their surfaces are repulsive and resistant to agglomeration.

As mentioned above, **DBT** served as the energy acceptor to capture excitation energy from **WP5**⊃**CPy** on account of their favorable energy-matching characteristics. As shown in Fig. 4a, the absorption spectrum of **DBT** exhibited significant overlap with the emission spectrum of **WP5**⊃**CPy**, facilitating efficient energy transfer between **WP5**⊃**CPy** and **DBT**. Upon the co-assembly of increasing **DBT** content, the fluorescence intensity of **WP5**⊃**CPy** at 460 nm decreased markedly, while the fluorescence peak of **DBT** at 580 nm continued to rise (Fig. 4b), indicative of the occurrence of energy transfer. Furthermore, a noticeable shift in fluorescence color from blue to orange was observed (Fig. 4c, inset). The FRET process was further corroborated by time-resolved fluorescence analysis. Fluorescence

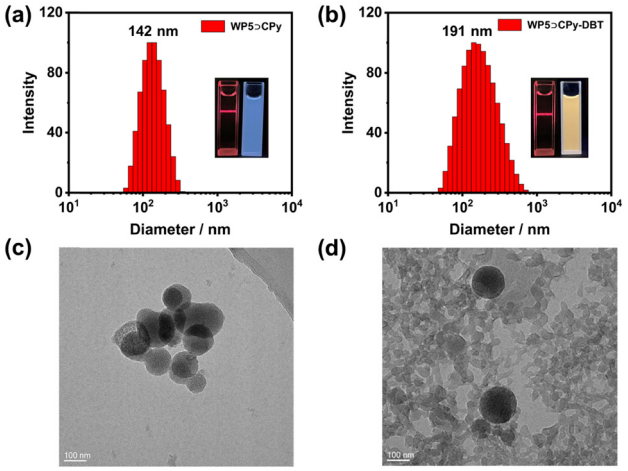

Fig. 3 DLS data of (a) **WP5⊃CPy** NPs (inset: Tyndall effect and fluorescence photograph of **WP5⊃CPy**), and (b) **WP5⊃CPy-DBT** NPs (inset: Tyndall effect and fluorescence photograph of **WP5⊃CPy-DBT**). TEM images of (c) **WP5⊃CPy** NPs and (d) **WP5⊃CPy-DBT** NPs. [**CPy**] = 5×10^{-5} M, [**WP5**] = 1.75×10^{-5} M, [**DBT**] = 2.5×10^{-7} M, respectively.

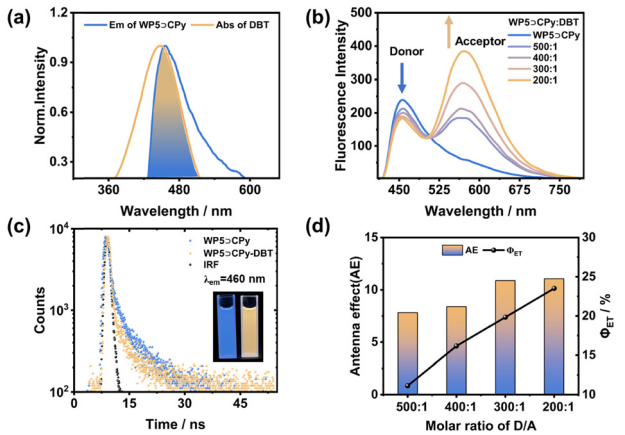

Fig. 4 (a) Normalized absorption and emission spectra of **WP5⊃CPy** (blue curve) and **DBT** (orange curve), respectively. (b) Fluorescence spectra of **WP5⊃CPy-DBT** in water at different donor/acceptor molar ratios. (c) Fluorescence decay profiles of **WP5⊃CPy** and **WP5⊃CPy-DBT**; inset: fluorescence photographs of **WP5⊃CPy** (left) and **WP5⊃CPy-DBT** (right). (d) Energy-transfer efficiency (Φ_{ET}) and antenna effect (AE) of the ALHS with varying acceptor content. [**CPy**] = 5×10^{-5} M, [**WP5**] = 1.75×10^{-5} M, [**DBT**] = 2.5×10^{-7} M, respectively.

lifetimes were fitted as a double exponential decay for both samples (Fig. 4c). The fluorescence lifetimes of **WP5⊃CPy** were determined to be τ_1 = 0.84 ns and τ_2 = 7.11 ns (Table S2, ESI†). In contrast, the fluorescence lifetimes of **WP5⊃CPy-DBT** decreased to τ_1 = 0.46 ns and τ_2 = 5.44 ns, providing additional evidence of light harvesting and energy transfer occurring within the nanoparticles.

To quantitatively assess the performance of the ALHS based on **WP5⊃CPy-DBT**, the energy transfer efficiency (Φ_{ET}) and antenna effect (AE) were systematically calculated. Φ_{ET} represents the ratio of the excitation energy absorbed by **DBT** to the

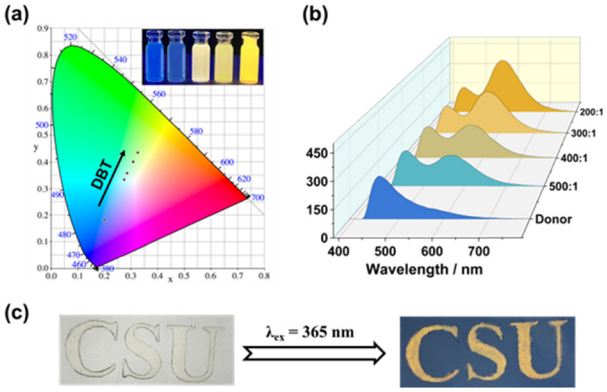

Fig. 5 (a) CIE chromaticity coordinates of **WP5⊃CPy** at various concentrations of **DBT**, accompanied by inset photographs displaying **WP5⊃CPy** NPs at different **DBT** concentrations under UV irradiation. (b) Fluorescence spectra of **WP5⊃CPy** in aqueous solution with varying concentrations of **DBT**. (c) Illustration of characters inscribed using a solution of **WP5⊃CPy-DBT** (D/A = 200/1), demonstrating its encryption function. Concentrations used in the experiments: [**CPy**] = 5×10^{-5} M, [**WP5**] = 1.75×10^{-5} M, [**DBT**] = 2.5×10^{-7} M, respectively.

total energy of **WP5⊃CPy**. Additionally, AE measures the emission amplification of **DBT** within the ALHS compared to its direct excitation. The resulting system exhibited enhanced energy transfer efficiency with increasing acceptor content (D/A = 500/1–200/1) (Fig. 4d). Φ_{ET} reaches 23.5% when D/A = 200/1 (Fig. S11 and Table S3, ESI†). Moreover, the system demonstrated considerable antenna effect values (7 to 11) at high D/A ratios (Fig. S12 and Table S4, ESI†). Furthermore, the absolute fluorescence quantum yield of the system increased from 2.72% (**WP5⊃CPy**) to 13.69% (**WP5⊃CPy-DBT**), indicative of a significant fluorescence enhancement through light harvesting (Fig. S10 and Table S1, ESI†). These quantitative findings collectively suggest that **WP5⊃CPy-DBT** represents an efficient supramolecular ALHS.

The dynamic characteristics of the **WP5⊃CPy-DBT** system confer upon it the ability to exhibit adjustable fluorescence colors. As depicted in the CIE 1931 chromaticity coordinates (Fig. 5a), the fluorescence emission color of the system varies with the molar ratio. Upon increasing the **DBT** content, the emission color of the system in water transitions gradually from blue to yellow. This transition is also evident in the fluorescence photograph of the samples (Fig. 5a, inset) and in the fluorescence spectra obtained through three-dimensional processing (Fig. 5b). Due to the system's AIE behavior, it displays luminescence not only in aqueous solution but also in the solid state. Upon inscription onto paper, characters rendered with the ALHS material remain unreadable under natural light but become clearly discernible under UV illumination, emitting a golden fluorescence color. This suggests the potential of the **WP5⊃CPy-DBT** system to serve as a customizable fluorescent encryption ink (Fig. 5c).

Conclusions

In summary, we have engineered an artificial light-harvesting system in aqueous solution through the host–guest interaction

between a pillar[5]arene host and a CS-based guest. The guest molecule, **CPy**, comprises a CS moiety and a methylpyridinium unit linked by a ten-carbon alkyl spacer, rendering it AIE active. Consequently, the water-soluble pillar[5]arene **WP5** induces the self-assembly of **CPy** into emissive nanoparticles, serving as an effective nano-platform and energy donor. Through the incorporation of the commercially available dye **DBT** into the supramolecular nanoparticles, we successfully constructed an efficient ALHS (**WP5⊃CPy-DBT**) based on FRET. The D/A ratio of the system is dynamically adjustable, leading to tunable fluorescence emission colors. Furthermore, these nanoparticles in aqueous solutions can serve as efficient solid-state information encryption materials due to their AIE properties. This study not only employs a straightforward supramolecular approach to fabricate an artificial light-harvesting system but also presents novel concepts for harnessing light energy and developing tunable luminescent materials.

Conflicts of interest

There are no conflicts to declare.

Acknowledgements

We gratefully acknowledge the National Natural Science Foundation of China (21702020), and The Analysis and Testing Center, NERC Biomass of Changzhou University is also acknowledged.

Notes and references

1 R. J. Sension, *Nature*, 2007, **446**, 740–741.
2 X. Qin, M. Suga, T. Kuang and J.-R. Shen, *Science*, 2015, **348**, 989–995.
3 T. Mirkovic, E. E. Ostroumov, J. M. Anna, R. van Grondelle, Govindjee and G. D. Scholes, *Chem. Rev.*, 2017, **117**, 249–293.
4 J. Otsuki, *J. Mater. Chem. A*, 2018, **6**, 6710–6753.
5 Z. Wu, H. Qian, X. Li, T. Xiao and L. Wang, *Chin. Chem. Lett.*, 2024, **35**, 108829.
6 D. Bokotial, K. Acharyya, A. Chowdhury and P. S. Mukherjee, *Angew. Chem., Int. Ed.*, 2024, **63**, e202401136.
7 X. M. Chen, X. Chen, X. F. Hou, S. Zhang, D. Chen and Q. Li, *Nanoscale Adv.*, 2023, **5**, 1830–1852.
8 K. Wang, K. Velmurugan, B. Li and X. Y. Hu, *Chem. Commun.*, 2021, **57**, 13641–13654.
9 T. Xiao, W. Zhong, L. Zhou, L. Xu, X.-Q. Sun, R. B. P. Elmes, X.-Y. Hu and L. Wang, *Chin. Chem. Lett.*, 2019, **30**, 31–36.
10 X.-Y. Dai, M. Huo and Y. Liu, *Nat. Rev. Chem.*, 2023, **7**, 854–874.
11 Z. Zhang, Z. Zhao, Y. Hou, H. Wang, X. Li, G. He and M. Zhang, *Angew. Chem., Int. Ed.*, 2019, **58**, 8862–8866.
12 M. Hao, G. Sun, M. Zuo, Z. Xu, Y. Chen, X. Y. Hu and L. Wang, *Angew. Chem., Int. Ed.*, 2020, **59**, 10095–10100.
13 P. P. Jia, L. Xu, Y. X. Hu, W. J. Li, X. Q. Wang, Q. H. Ling, X. Shi, G. Q. Yin, X. Li, H. Sun, Y. Jiang and H. B. Yang, *J. Am. Chem. Soc.*, 2021, **143**, 399–408.
14 D. Zhang, W. Yu, S. Li, Y. Xia, X. Li, Y. Li and T. Yi, *J. Am. Chem. Soc.*, 2021, **143**, 1313–1317.
15 Y. Li, C. Xia, R. Tian, L. Zhao, J. Hou, J. Wang, Q. Luo, J. Xu, L. Wang, C. Hou, B. Yang, H. Sun and J. Liu, *ACS Nano*, 2022, **16**, 8012–8021.
16 G. Sun, M. Li, L. Cai, D. Wang, Y. Cui, Y. Hu, T. Sun, J. Zhu and Y. Tang, *J. Colloid Interface Sci.*, 2023, **641**, 803–811.
17 Y. Wang, C. Q. Ma, X. L. Li, R. Z. Dong, H. Liu, R. Z. Wang, S. S. Yu and L. B. Xing, *J. Mater. Chem. A*, 2023, **11**, 2627–2633.
18 T. Xiao, D. Chen, H. Qian, Y. Shen, L. Zhang, Z.-Y. Li and X.-Q. Sun, *Dyes Pigm.*, 2023, **210**, 110958.
19 Z. Xu, S. Peng, Y. Y. Wang, J. K. Zhang, I. Lazar Alexandra and D. S. Guo, *Adv. Mater.*, 2016, **28**, 7666–7671.
20 L. Ji, Y. Sang, G. Ouyang, D. Yang, P. Duan, Y. Jiang and M. Liu, *Angew. Chem., Int. Ed.*, 2019, **58**, 844–848.
21 X. H. Wang, N. Song, W. Hou, C. Y. Wang, Y. Wang, J. Tang and Y. W. Yang, *Adv. Mater.*, 2019, **31**, e1903962.
22 L. Xu, Z. Wang, R. Wang, L. Wang, X. He, H. Jiang, H. Tang, D. Cao and B. Z. Tang, *Angew. Chem., Int. Ed.*, 2020, **59**, 9908–9913.
23 Q. Song, S. Goia, J. Yang, S. C. L. Hall, M. Staniforth, V. G. Stavros and S. Perrier, *J. Am. Chem. Soc.*, 2021, **143**, 382–389.
24 Y. Han, X. Zhang, Z. Ge, Z. Gao, R. Liao and F. Wang, *Nat. Commun.*, 2022, **13**, 3546.
25 Z. Lian, J. He, L. Liu, Y. Fan, X. Chen and H. Jiang, *Nat. Commun.*, 2023, **14**, 2752.
26 B. Shi, P. Qin, W. Li, H. Feng, Y. Zhou, Y. Chai, W.-J. Qu, T.-B. Wei, Y.-M. Zhang and Q. Lin, *Inorg. Chem.*, 2023, **62**, 17236–17240.
27 M. D. Tian, Z. Wang, X. Yuan, H. Zhang, Z. X. Liu and Y. Liu, *Adv. Funct. Mater.*, 2023, **33**, 2300779.
28 T. Xiao, H. Qian, X. Li, Z. Wu, Z.-Y. Li and X.-Q. Sun, *Dyes Pigm.*, 2023, **215**, 111289.
29 D. Jia, H. Zhong, S. Jiang, R. Yao and F. Wang, *Chin. Chem. Lett.*, 2022, **33**, 4900–4903.
30 J.-L. Yu, Z. Chen, Y.-Q. Zhu, Y.-L. Jin, X. Wang, M.-X. Wu, X.-H. Wang and Y.-W. Yang, *Aggregate*, 2024, **5**, e562.
31 T. Xiao, C. Bao, L. Zhang, K. Diao, D. Ren, C. Wei, Z.-Y. Li and X.-Q. Sun, *J. Mater. Chem. A*, 2022, **10**, 8528–8534.
32 X. Ma, T. Ren, J. Tang, J. Zhang, J. Wei, Y. Liang, J. Zhang, E. Feng and X. Han, *ChemistrySelect*, 2024, **9**, e202304171.
33 Z. Wu, Q. Zhang, D. Chen and T. Xiao, *Sens. Diagn.*, 2024, **3**, 295–300.
34 X. M. Chen, Q. Cao, H. K. Bisoyi, M. Wang, H. Yang and Q. Li, *Angew. Chem., Int. Ed.*, 2020, **59**, 10493–10497.
35 K.-X. Teng, Z.-P. An, L.-Y. Niu and Q.-Z. Yang, *ACS Mater. Lett.*, 2023, **6**, 290–297.
36 X. Q. Tian, S. K. Li, K. Velmurugan, Z. H. Bai, Q. Liu, K. Y. Wang, M. Z. Zuo and X. Y. Hu, *Mater. Chem. Front.*, 2023, **7**, 2484–2492.
37 Z. Wang, X. He, T. Yong, Y. Miao, C. Zhang and B. Zhong Tang, *J. Am. Chem. Soc.*, 2020, **142**, 512–519.

38 R. Biswas and S. Banerjee, *J. Phys. Chem. B*, 2023, **127**, 4135–4144.
39 T. Xiao, D. Ren, L. Tang, Z. Wu, Q. Wang, Z.-Y. Li and X.-Q. Sun, *J. Mater. Chem. A*, 2023, **11**, 18419–18425.
40 T. Xiao, L. Tang, D. Ren, K. Diao, Z.-Y. Li and X.-Q. Sun, *Chem. – Eur. J.*, 2023, **29**, e202203463.
41 L. Tang, Z. Wu, Q. Zhang, Q. Hu, X. Dang, F. Cui, L. Tang and T. Xiao, *Chem. Commun.*, 2024, **60**, 4719–4722.
42 T. Xiao, X. Wei, H. Wu, K. Diao, Z.-Y. Li and X.-Q. Sun, *Dyes Pigm.*, 2021, **188**, 109161.
43 T. Xiao, H. Qian, Y. Shen, C. Wei, D. Ren, L. Zhang, Z. Y. Li, L. Wang and X. Q. Sun, *Mater. Today Chem.*, 2022, **24**, 100833.
44 B. Mu, X. Hao, X. Luo, Z. Yang, H. Lu and W. Tian, *Nat. Commun.*, 2024, **15**, 903.
45 K. Zhong, S. Lu, W. Guo, J. Su, S. Sun, J. Hai and B. Wang, *Chem. Commun.*, 2021, **57**, 9434–9437.
46 T. Xiao, L. Zhang, D. Chen, Q. Zhang, Q. Wang, Z.-Y. Li and X.-Q. Sun, *Org. Chem. Front.*, 2023, **10**, 3245–3251.
47 B. Sk and S. Hirata, *Chem. Commun.*, 2023, **59**, 6643–6659.
48 L. Wu, C. Huang, B. P. Emery, A. C. Sedgwick, S. D. Bull, X.-P. He, H. Tian, J. Yoon, J. L. Sessler and T. D. James, *Chem. Soc. Rev.*, 2020, **49**, 5110–5139.
49 R. M. Clegg, *Cur. Opin. Biotech.*, 1995, **6**, 103–110.
50 S. Guo, Y. Song, Y. He, X. Y. Hu and L. Wang, *Angew. Chem., Int. Ed.*, 2018, **57**, 3163–3167.
51 F. Würthner, *Angew. Chem., Int. Ed.*, 2020, **59**, 14192–14196.
52 Y. Hong, J. W. Y. Lam and B. Z. Tang, *Chem. Soc. Rev.*, 2011, **40**, 5361–5388.
53 X.-Y. Lou, G. Zhang, N. Song and Y.-W. Yang, *Biomaterials*, 2022, **286**, 121595.
54 Y.-X. Hu, W.-J. Li, P.-P. Jia, X.-Q. Wang, L. Xu and H.-B. Yang, *Adv. Opt. Mater.*, 2020, **8**, 2000265.
55 X. Tang, Y. Zhu, W. Guan and C. Lu, *Aggregate*, 2023, **4**, e348.
56 X. Y. Lou and Y. W. Yang, *Aggregate*, 2020, **1**, 19–30.
57 X. Y. Lou and Y. W. Yang, *Adv. Opt. Mater.*, 2018, **6**, 1800668.
58 D. Ren, L. Tang, Z. Wu, Q. Zhang, T. Xiao, R. B. P. Elmes and L. Wang, *Chin. Chem. Lett.*, 2023, **34**, 108617.
59 Y. L. Ding, J. Guo, X. He, W. Tao, Y. D. Shi, J. H. Xu, L. Xu, M. X. Tang, D. K. Shen, H. Bi, Z. Q. Wu, K. Yang, Z. B. Zeng and P. F. Wei, *Adv. Funct. Mater.*, 2023, **33**, 2212886.
60 H. Wu and T. Xiao, *Front. Chem.*, 2020, **8**, 610093.
61 H.-J. Kim, P. C. Nandajan, J. Gierschner and S. Y. Park, *Adv. Funct. Mater.*, 2018, **28**, 1705141.
62 Y. Zhang, Y. Xue, L. Gao, R. Liao, F. Wang and F. Wang, *Chin. Chem. Lett.*, 2024, **35**, 109217.
63 T. Xiao, X. Li, L. Zhang, K. Diao, Z.-Y. Li, X.-Q. Sun and L. Wang, *Chin. Chem. Lett.*, 2024, **35**, 108618.
64 X. H. Wang, X. Y. Lou, T. Lu, C. Wang, J. Tang, F. Liu, Y. Wang and Y. W. Yang, *ACS Appl. Mater. Interfaces*, 2021, **13**, 4593–4604.
65 D. Chen, C. Bao, L. Zhang, Q. Zhang, Z. Wu, Z.-Y. Li, X.-Q. Sun, L. Wang and T. Xiao, *Adv. Funct. Mater.*, 2024, **34**, 2314093.
66 K. Diao, D. J. Whitaker, Z. Huang, H. Qian, D. Ren, L. Zhang, Z.-Y. Li, X.-Q. Sun, T. Xiao and L. Wang, *Chem. Commun.*, 2022, **58**, 2343–2346.
67 T. Ogoshi, T.-a Yamagishi and Y. Nakamoto, *Chem. Rev.*, 2016, **116**, 7937–8002.
68 M. Xue, Y. Yang, X. Chi, Z. Zhang and F. Huang, *Acc. Chem. Res.*, 2012, **45**, 1294–1308.
69 T. Xiao, L. Zhou, L. Xu, W. Zhong, W. Zhao, X.-Q. Sun and R. B. P. Elmes, *Chin. Chem. Lett.*, 2019, **30**, 271–276.
70 H. Zheng, L. Fu, R. Wang, J. Jiao, Y. Song, C. Shi, Y. Chen, J. Jiang, C. Lin, J. Ma and L. Wang, *Nat. Commun.*, 2023, **14**, 590.
71 C. Ding, Y. Liu, T. Wang and J. Fu, *J. Mater. Chem. B*, 2016, **4**, 2819–2827.
72 G. Sun, W. Qian, J. Jiao, T. Han, Y. Shi, X.-Y. Hu and L. Wang, *J. Mater. Chem. A*, 2020, **8**, 9590–9596.